Unlock your experimental potential with power and agility

Busy labs like yours require flexibility and greater resolution to stay a step ahead and adapt to ever-evolving flow cytometry research needs. That's why we've specially designed the BD FACSymphony™ A5 SE Cell Analyzer to give you the power of spectral technology with the added flexibility to choose between spectral unmixing or compensation workflows.

With the BD FACSymphony™ A5 SE Cell Analyzer, you can support varying user preferences and assay requirements all from one platform.

You don't have to compromise power for agility–now you can have both.

Expand your experimental power.

Discover the difference at **bdbiosciences.com/se**

BD

Cytometry PART A
Journal of Quantitative Cell Science

Quantification of Alignment of Vascular Smooth Muscle Cells

Marcel P. Dorta,[1] Isis V. de Brito,[1] Alexandre C. Pereira,[2] Adriano M. Alencar[1]*

[1]Laboratory of Microrheology and Molecular Physiology, Department of General Physics, Physics Institute, University of São Paulo, São Paulo, Brazil

[2]Laboratory of Genetics and Molecular Cardiology, Department of Cardiology, Heart Institute, Medical School, University of São Paulo, São Paulo, Brazil

Received 25 September 2017; Revised 5 February 2018; Accepted 13 February 2018

Grant sponsor: Fundação de Amparo à Pesquisa do Estado de São Paulo (FAPESP), Grant number: 2012/07059–8, 2014/21646–9, and 2014/22102–2

Additional Supporting Information may be found in the online version of this article.

*Correspondence to: Adriano M. Alencar, Instituto de Física, Rua do Matão 1371, travessa R. 05508-090, São Paulo/SP, Brazil. Email: aalencar@usp.br

Published online 26 March 2018 in Wiley Online Library (wileyonlinelibrary.com)

DOI: 10.1002/cyto.a.23355

Abstract

Vascular smooth muscle cells (VSMCs) are essential components that keep the tonus of the arterial network, which is the channel used to conduct the blood from the heart to the peripheral areas of the body. It is known that mechanical and architectural changes in VSMCs may lead to functional modifications in the cardiovascular system; therefore, the quantitative characterization of these changes can help to elucidate questions that remain unclear in pathological situations, such as hypertension, vasospasm, vascular hypertrophy, and atherosclerosis. In this work, we have developed a new framework of image processing using the Sobel operator, associated with statistical analysis, to determine the degree of local alignment of actin filaments, which we found to be directly related with the distensibility of the arterial wall. We have also compared these results with the rigidity of the cytoskeleton of VSMCs. The results suggest that the alignment degree increases from peripheral arteries, such as carotid and femoral, to central arteries, as well coronary and thoracic aorta, which can indicate that the level of local alignment of the actin fibers in VSMCs is related with the mechanical behavior of the arterial wall. © 2018 International Society for Advancement of Cytometry

Key terms

F-actin; Kurtosis; arterial tonus; rheology; viscoelasticity

THE smooth muscle cells (SMCs) control the tonus of hollow organs of the mammalians body. Specifically, for vessels and arteries, the vascular SMCs (VSMCs) contributes to the mechanical properties of the vascular system (1), which is critical for their main functions, such as, contraction, blood pressure regulation, and blood flow distribution (2). The VSMCs also present a singular plasticity, and can exhibit phenotypic changes in response to environmental or physiological stimulus (3,4). In applied research, it has been shown that the VSMC mechanical properties present a significant intraindividual and interindividual variation (5,6), anomalous and quake-like dynamics (7). These behaviors are mainly determined by the cytoskeleton, mostly through actin filaments, which also defines the cell architecture (8–10). Therefore, the only way to fully understand the relationship between the structure of VSMCs and mechanical behavior of the arterial system goes through the characterization of the cytoskeleton (F-actin) organization (11). Thus, we have developed a set of tools to analyze images of VSMCs to perform this characterization, associating the results with the distensibility of the arterial wall and with the stiffness of the cytoskeleton of these cells.

Advanced fluorescence and optical methods associated with image processing techniques have been used to analyze structural changes associated with the reorganization of the F-actin (12). In general, the raw digital images from biological samples must be preprocessed to suppress imperfections, artifacts from the acquisition process and undesired noise background, or to enhance some important features for further processing (13). Following this step, depending on the scientific question, the processing itself varies hugely, leading to the use of a significant amount of different

ISAC International Society for Advancement of Cytometry

analytical techniques, such as methods based on fast Fourier transform (FFT) and the edge identification by Sobel operator. Specifically, these can be used as cell image processing techniques to quantify the alignment of the intracellular fibers (14–16). These two methods were compared in the work of Kemeny and Clyne (17), in which they have shown that edge detection methods, such the Sobel operator, are more sensitive than FFT methods.

In the works of Yoshigi et al. (14), image processing algorithms were used to calculate the degree of cytoskeleton fiber alignment of vascular endothelial cells, expressing the results of variance and Kurtosis of F-actin distribution angle. Based on this work, we have developed a novel VSMC image analysis platform composed of specific functions, organized in an algorithm that aims to quantify the degree of alignment (DA) of F-actin in VSMC's. Our image-processing platform uses the Sobel operator to identify the borders of the F-actin and calculate the angle per pixel. The alignment of F-actin in several small regions of the image is estimated by determining the Kurtosis of the angle distribution for each region (14,17). To demonstrate the application possibilities of our method we have calculated the DA of fibers of VSMCs, using images of cells obtained from different porcine arterial beds (5). We have hypothesized that the structural properties, such as the alignment of the F-actin, can determine the organization of the whole VSMC, and can also be related to the elastic behavior of the arterial wall. Thus, based on this hypothesis, we have compared our results with mechanical parameters of these two arterial elements: the viscoelasticity of the cytoskeleton of VSMCs (5) and the pressure-strain elastic modulus (E_P), obtained from the literature (18,19). This is a parameter that relates pressure and diameter changes during the systole and diastole cycle (19). Through our analysis, we have shown that, the parameters that characterize the F-actin organization of VSMCs can be related to the mechanical behavior of the arterial wall, but they did not show a good correspondence with the stiffness of the cytoskeleton of these cells.

Methodological Developments

Detailed descriptions of the cell culture and isolation are reported elsewhere (5). Briefly, fragments of abdominal aorta, femoral, renal, carotid, coronary, and thoracic aorta arteries were collected from five pigs to isolate VSMCs using the primary explant technique. The cells were either fixed and incubated with phalloidin conjugated with Alexa (1:400; Alexa Fluor 488 Phalloidin; Invitrogen) or for 12 h with anti-vinculin primary antibody (1:200; catalog no. V9131; Sigma-Aldrich). In the latter case, followed by 2 h incubation with anti-mouse secondary antibody (Alexa Fluor 555 goat anti-mouse IgG, 1:500; Invitrogen). Confocal images were acquired using a Zeiss laser-scanning confocal microscope LSM 510 META using the 20x objective lens (Plan-Apo/0.75 NA) (5,20). The emission filter bandwidth is 505–550 nm with the center at 518 nm. The procedure was approved according to our local ethics committee (CAPpesq–Hospital das Clínicas da Faculdade de Medicina USP-0272/11).

Preprocessing and Analysis

The confocal system generates a LSM file format, which is an extended multi page TIFF-format that can hold few standard TIFF data channels, usually one image per dye. Here, we only need the channel tailored to visualize F-actin. Our analysis platform was built in Matlab® and was based on three main steps: in the first, we preprocess uncompressed TIFF (8 bits, 512 × 512 pixels) confocal images of vascular smooth muscle cells (VSMCs) (14,17), then we apply an algorithm of edge detection and calculate the DA using the methodology that will be summarized here. For each arterial bed, we used a set of six images.

During the preprocessing, the data of the F-actin labeled fluorescence images were adjusted, improving the contrast of the actin fibers: we used a generalization of the Otsu method to eliminate the image background noise, which is widely used for this purpose (17,21–25). That method establishes an optimum threshold L_c, however, often, due the experimental setup, the noise and the signal are too close and the threshold L_c may not be the best choice. This is the case of our images where the pure Otsu method generated a very high L_c (Fig. 1B). Thus, to overcome this difficulty, but keeping a user independent threshold selection, we applied a single correction factor for all images, $L_{cg}=\alpha L_c$, where here, $\alpha=0.3$, which eliminates most of the noise, keeping the information from the fibers (Fig. 1C).

Quantification of the DA

To quantify the DA, the Sobel operator was used, adopting the methodological procedures described by Yoshigui et al. (14). Given a gray scale image, this operator calculates the brightness of each pixel $P_{i,j}$, where i and j represent the coordinates of the pixel, of an image using the following horizontal and vertical convolution matrixes:

$$M_h=\begin{pmatrix}-1 & 0 & 1\\ -2 & 0 & 2\\ -1 & 0 & 1\end{pmatrix}, \tag{1}$$

$$M_v=\begin{pmatrix}-1 & -2 & -1\\ 0 & 0 & 0\\ 1 & 2 & 1\end{pmatrix}, \tag{2}$$

where M_h and M_v represent, respectively, the magnitude of the brightness gradient in horizontal and vertical directions. The neighbors of each pixel were selected as a sample matrix $S_{i,j}$:

$$S_{i,j}=\begin{pmatrix}P_{i-1,j-1} & P_{i-1,j} & P_{i-1,j+1}\\ P_{i,j-1} & P_{i,j} & P_{i,j+1}\\ P_{i+1,j-1} & P_{i+1,j} & P_{i+1,j+1}\end{pmatrix}. \tag{3}$$

Thus, during image analysis, the horizontal (H_h) and vertical (H_v) convolutions were calculated using the following expressions:

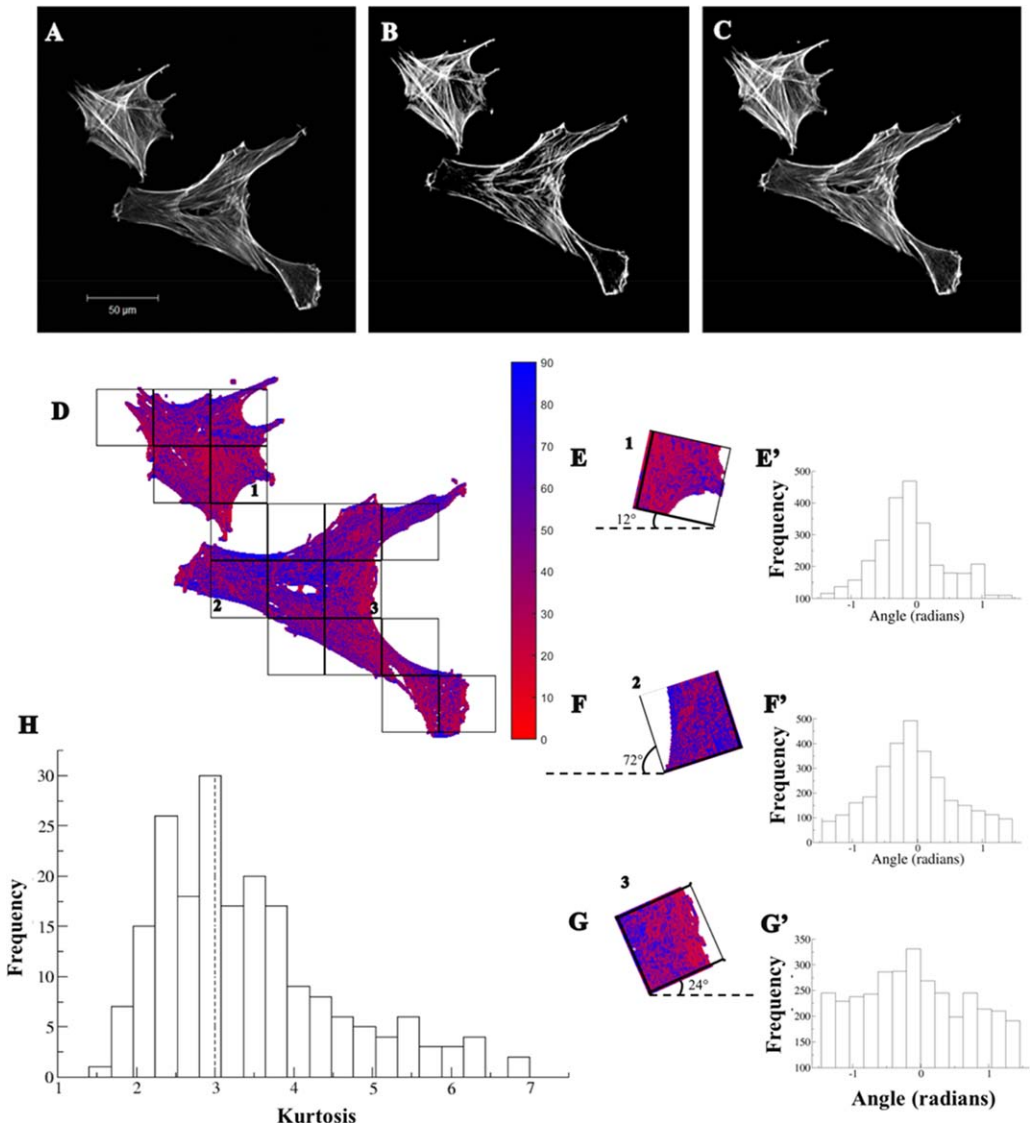

Figure 1. Quantification of the degree of alignment of actin fibers of VSMCs using statistical analysis. We applied a generalization of the Otsu method to improve the contrast of our fluorescence labeled images (**A**). In **B**, we have an image adjusted by an optimal threshold (L_c) determined by the Otsu's traditional method, which applied a very high L_c. To overcome this problem, we applied the condition $L_{cg}=\alpha L_c$, where $\alpha=0.3$ (**C**). **D**: Grayscale (or online color) coded image representing the angles per pixel of thoracic aorta divided in16 $\times$ 16 squared windows. The grayscale version's (color code) was implemented to differentiate the orientation angles for each pixel: for angles closer to $\pi/2$ rad, the pixel fibers' shades were white (blue) and for angles closer to 0 rad, pixel fibers' shades were black (red). From **F** to **G**: Rotation of the preferential angle to zero in local regions numbered from 1 to 3. From **F'** to **G'**: Histograms of the angles for each local region, after the rotation. **H**: Histogram of the Kurtosis for all the local regions in the image presented in **D**. A dotted line for $K=3$ indicates the region where the integral of the Eq. (8) is applied, after a normalization, to evaluate the degree of alignment of the cells. [Color figure can be viewed at wileyonlinelibrary.com]

$$H_h(i,j)=\sum M_h \cdot S_{i,j}, \tag{4}$$

$$H_v(i,j)=\sum M_v \cdot S_{i,j}. \tag{5}$$

The values of $H_h(i,j)$ and $H_v(i,j)$ represent the magnitude of the brightness gradient along the horizontal and vertical directions, respectively. The angle (θ) for each pixel was calculated using the arctangent function:

$$\theta(i,j)=\arctan\left(\frac{H_v}{H_h}\right). \tag{6}$$

Subsequently, a color-coding scheme was used to facilitate the characterization of the fibers directions. To simplify the interpretation, the orientation angles of the fibers have been adjusted between $-\pi/2$ and $\pi/2$ rad (Fig. 1D). By calculating the angle per pixel, using Eq. (6), and building its histogram, we could find the preferential angle. However, we note that, although the fibers of the cell are aligned in clusterized regions, those regions are not aligned to one another, tending to the global alignment vanishes. Thus, we divided the whole image in a set of $0 > n > N$ small regions with $L \times L$ pixels,

calculated the angle probability distributions of all regions, $\Pi_n(\theta)$, identifying the position of the peak of $\Pi_n(\theta)$, which we assigned to be the preferential orientation of *n*. We choose the size *L* of these regions, so it could capture the alignment clusters. We rotated each subregion aiming that the preferential orientation becomes zero centered and the angles are redistributed to be between $-\pi/2$ and $\pi/2$ rad (see Figs. 1E–1G). Then we called DA the dispersion of the distribution around zero by calculating the Kurtosis, $K[\Pi_n(\theta)]$, which is known to be a good descriptor of the shape of the distribution, which is given by:

$$K[\Pi_n(\theta)] = \frac{1}{L2}\frac{\left[\sum_{i,j}\left(\theta(i,j)-\bar{\theta}\right)^4\right]}{\left(\sigma^2\right)^2}, \qquad (7)$$

where $\bar{\theta}$ is the sample mean and σ is the standard deviation of $\theta(i,j)$. Normal distributions have values of$K$ $[\Pi_n(\theta)]=3$,-while peaked distributions have $K[\Pi_n(\theta)] > 3$, as can be seen in Figure 1E', and are considered highly aligned subregions. Distributions with $K[\Pi_n(\theta)] < 3$ are flatter distributions with high dispersion, as can be seen in Figure 1G', and are considered regions with low DA. Thus, values of *K* between 3 and ∞ characterize regions that are considered aligned. We obtained the probability distribution of the Kurtosis $\Pi(K)$ for the *N* subregions, by normalizing its histogram (Figure 1H) by the total area, as $\int_0^\infty \Pi(K)dK=1$. Finally, we defined the DA as:

$$\mathrm{DA}=\int_3^\infty \Pi(K)\,dK\,. \qquad (8)$$

We applied this methodology for different values of *L*, $8 \le L \le 32$ pixels, and they did not show significant variation, thus, we adopted L =16 as the window size because the average standard deviation of the DA was lower than the other sizes (Fig. 2B). Furthermore, this size showed to be more efficient to cover appropriately the images of the cells (Fig. 2E). Larger windows will include too much background (in Figs. 2C and 2D), while smaller windows will include only few fibers.

Results and Discussion

Figures 3A and 3B show two images of VSMCs obtained from carotid and coronary arteries using fluorescence confocal microscope. From these images, which are from the same animal, one can notice a shape difference, but standard methods to measure the alignment are not able to detect differences.

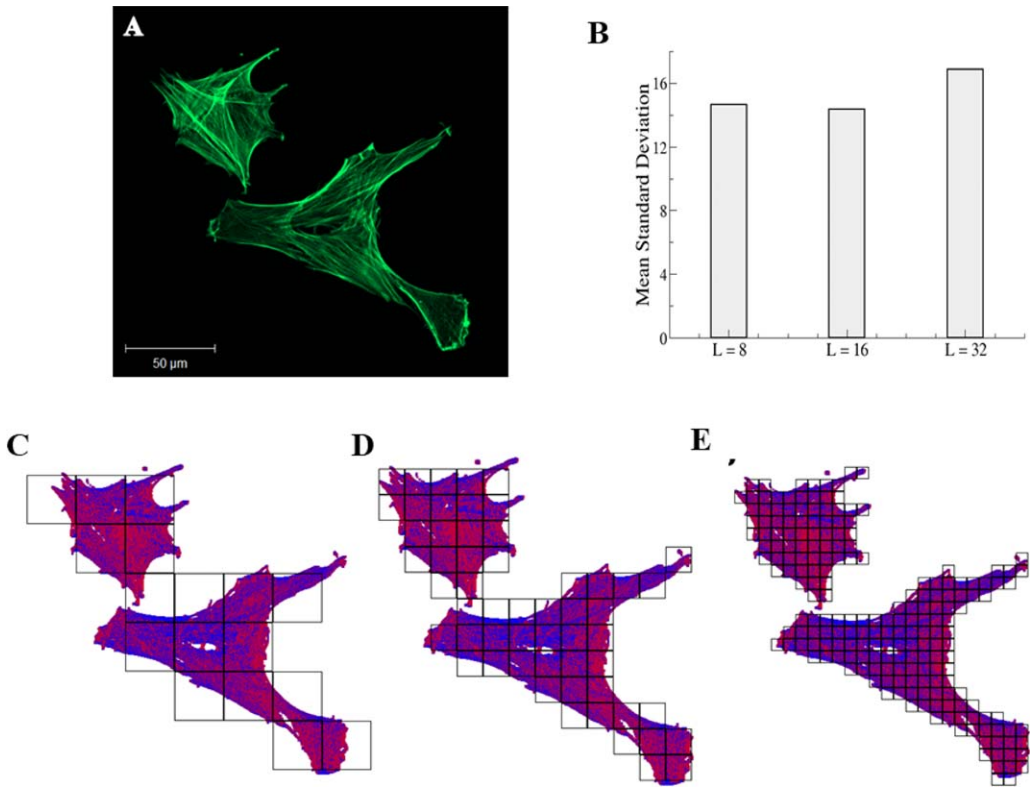

Figure 2. Cell imaging processing **A**: Fluorescence microscopy image of two VSMCs obtained from a porcine thoracic aorta using the methodology described previously. Samples were stained with phalloidin. Different windows sizes (**C**: 64, **D**: 32, and **E**: 16) were used to divide VSMCs images to calculate the degree of local alignment of the F-actin. Using six images, for each one of the six different arterial beds (femoral, carotid, thoracic aorta, abdominal aorta, coronary, and renal artery) used in this work, the degree of local alignment was estimated, and we decided to adopt $L = 16$, because the results obtained using this window size showed a smaller mean standard deviation of the values of DA (**B**). As we can see from the picture, this window size is suitable for our purpose, because it covers almost the entire cell, reducing background regions and covering a number of fibers enough to generate reliable results. Note that, the size of *L* has to change once the magnification used to take the images changes. [Color figure can be viewed at wileyonlinelibrary.com]

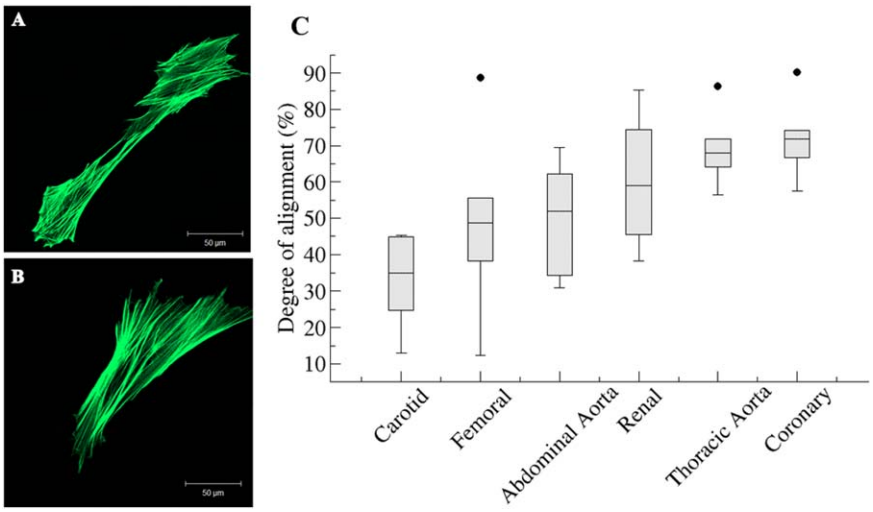

Figure 3. DA for VSMCs collected from different porcine arterial beds. The arteries are organized in a sequence: from peripheral to central arteries. Fluorescence confocal images of **A**: thoracic aorta VSMCs and **B**: femoral VSMCs stained with phalloidin. The images indicate that the cells present different shape and alignment of the actin fibers. This difference may have influence on the mechanical behavior of the cells and, as a consequence, it may be related to the mechanical behavior of the arterial wall. **C**: Box plot of the DA (%) for VSMCs from each arterial bed, where the dots are outliers. This result indicates that peripheral arteries presented more aligned cells than the central arteries, when we consider central arteries the ones that are closest to the heart and peripheral as the arteries near the extremities of the animal body (head and members). [Color figure can be viewed at wileyonlinelibrary.com]

However, using our previously described method, we can quantify the differences in the alignment of the internal fibers, as we can see in the box plot of the DA for six different arterial beds (Fig. 3C). It shows that peripheral vessels, such as carotid and femoral arteries(18), displayed lower DA values (32.9% and 48.7%, respectively) than the cells from central vessels, as thoracic and coronary artery (69.1% and 72%, respectively).

We have shown that the DA VSMC changes obtained from different regions of the arterial tree, increase from peripheral to central arteries, which may indicate that the structure of the VSMCs changes to be adapted to the arterial function. With the same idea in mind, several authors studied the mechanical properties of vessels (5,18–20,26,27), such as Dinardo et al. (5), who showed that the VSMC rigidity, from the same set of images used here, increases as their vessel of origin moves away from the heart. These parameters were evaluated using optical magnetic twisting cytometry (OMTC) and our data of DA were plotted together for comparison. The Figure 4 shows the *Z*-score, or rigidity, from the apparent stiffness (G) versus the DA of the VSMCs. Here, the arterial beds were distributed in the x-axis, from the peripheral to central arteries. The rigidity shows a small fluctuation between the arterial beds, without a clear trend, while the DA increases. This difference can show that the rigidity of the cytoskeleton may not be influenced by the local alignment of the F-actin.

However, we observed that, among anatomical and structural parameters of vessels obtained from the literature (5,18,19,28), such as media thickness, internal diameter, thickness/internal diameter, percentage of collagen and percentage of elastin, the arterial wall distensibility is the parameter that best correlates with DA. The distensibility is the inverse of the pressure-strain elastic modulus (E_P), as described by Slørdahl et al. (28). In this work, the authors evaluated the E_P of central arteries and show that the E_P, from pig's central arteries, increase with the distance from the heart. From their results, we calculated the distensibility as the inverse of E_P for four different arterial beds in the aorta (ascending aorta, descending aorta, abdominal aorta high, and abdominal aorta low) and compared with our DA results, also from pigs (Fig. 3C), as is shown in Figure 5.

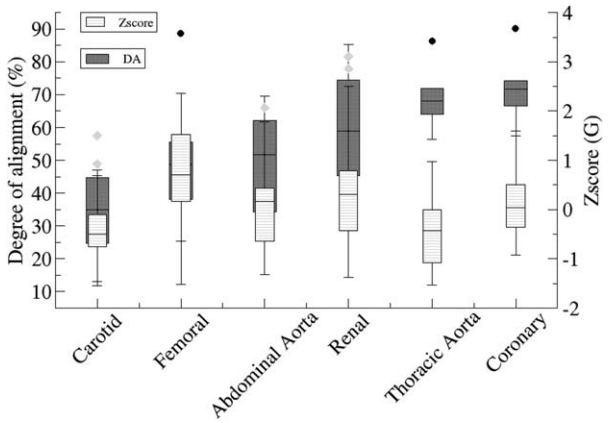

Figure 4. Box plot (light gray) representing the *Z*-scores of the variable G for each artery which indicates the VSMC rigidity according to the position in the arterial tree. This box plot was adapted from the original data obtained by Dinardo et al. (5). Here, we just changed the sequence of the arterial beds. The box plot of the DA (dark gray) is plotted with the *Z*-score for comparison. These graphs indicate that the alignment of the F-actin of VSMCs can be related with the mechanical behavior of the arterial wall, but it did not show a correlation with the rigidity of the VSMC cytoskeleton.

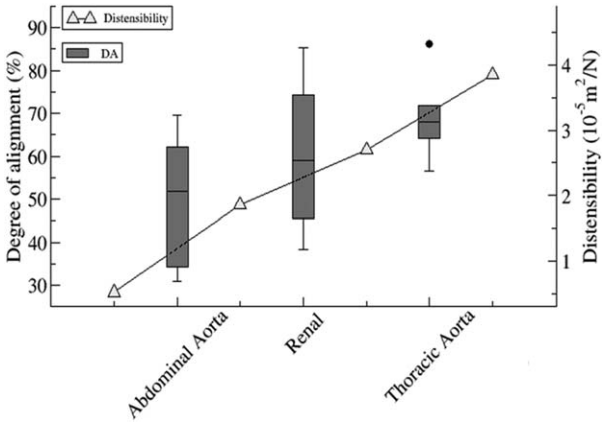

Figure 5. Comparison between our results and the data obtained by Slørdahl et al. (28) for four different arterial beds at the aorta of a set of six pigs (ascending aorta, descending aorta, abdominal aorta high, and abdominal aorta low). The arterial beds are distributed in the graph's axis as they are located in the animal's body. The box plot represents the data obtained in this work and the triangles represent the literature data.

Similar studies also shows that the arterial wall distensibility increases from peripheral to central arteries for dogs, Peterson et al. (19), and sheep, Mangell et al. (18). Thus, all of them agree that the three species follows the same tendency. In Figure 6, we extrapolate our results of VSMCs DA from pig (arterial beds: carotid, femoral, abdominal aorta and thoracic aorta) to compare against the distensibility of the arterial wall among different species, dog (19) and sheep (18). We can see that, for all the three species the distensibility and DA increases from peripheral to central arteries. Hence, from our data, we found that cells in arterial beds with more capacity of distension present more stress fibers aligned. We could, again, extrapolate our findings considering that the blood flow shear stress play an important role in arterial distensibility (29). Thus, the cell stress fibers alignment may be a consequence of the shear stress. If this is true, it can be used to couple macroscopic mechanical parameters with the microscopic cell structure.

Here, we have developed an innovative, user independent, and automated methodology for image analysis, which covers an important structural property of cells: the DA. We hypothesized that this parameter can be defined by the orientation of the actin fibers, which is a determinant element for the elastic behavior of the cardiovascular system. We applied our platform to perform a statistical analysis of images of vascular smooth muscle cells obtained from several segments collected from a porcine arterial tree. Our method showed to be efficient for determining the DA of VSMCs, since it enabled quantitative and fast analysis of the alignment of the fibers in local regions of the cells.

The methodology applied here was different from others, such as the one presented by Yoshigi et al. (14), and of Kemeny et al. (17), once we are not determining the preferential angle of the actin fibers, but the degree of local alignment. While our method is focusing on the individual cell properties, which may be directly related to the viscoelasticity and phenotype cell adaptation, the method suggested by Yoshigi et al. is focusing, for instance, on the collective and preferential alignment of a confluent group of cells forming a monolayer and under unidirectional mechanical stress. Thus, it is not possible to identify if the cytoskeleton of a given cell is more or less aligned than the cytoskeleton of another cell.

Our method can be used to any type of fiber inside a cell, as microtubules and intermediate filaments and can also be applied to human VSMCs or other human cells. However, the method needs to adopt a specific window size, which should be tested before processing the data, since the relative size of the cells varies from one experimental setup to another. The size of the window cannot reach the size of the cell, as well as, it cannot be too small. Thus, we found that the window size should be between 1/10 and 1/40 of the total cell length, in pixels. Another limitation was imposed by the image acquisition process, since focus adjustment of the image and fading of fluorochromes influenced the contrast of the fiber image. Despite these limitations, our method proved to be efficient to determine the degree of alignment of VSMCs and can be used to characterize the cell in different studies.

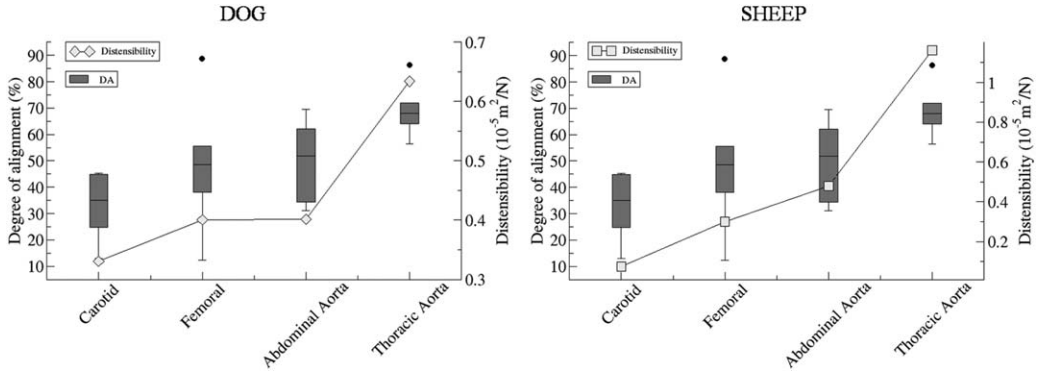

Figure 6. DA of VSMCs calculated from different porcine arterial beds compared with the inverse of pressure-strain elastic modulus (distensibility) of arteries for dog (diamonds) and sheep (squares) (19). It's been found modulus of thoracic aorta, abdominal aorta, femoral, and carotid arteries, but modules of renal and coronary arteries of the same animal were not found for comparison.

Literature Cited

1. Wagenseil JE, Mecham RP. Vascular extracellular matrix and arterial mechanics. Physiol Rev 2009;89:957–989. Available at: http://physrev.physiology.org/cgi/doi/10.1152/physrev.00041.2008
2. Owens GK, Kumar MS, Wamhoff BR. Molecular regulation of vascular smooth muscle cell differentiation in development and disease. Physiol Rev 2004;84:767–801. Available at: http://www.ncbi.nlm.nih.gov/pubmed/15269336 (accessed on January 23, 2014).
3. Rzucidlo EM, Martin KA, Powell RJ. Regulation of vascular smooth muscle cell differentiation. J Vasc Surg 2007;45(Suppl. A):A25–A32. Available at: http://www.ncbi.nlm.nih.gov/pubmed/17544021 (accessed on February 17, 2014).
4. Seriani R, de Souza CEC, Krempel PG, Frias DP, Matsuda M, Correia AT, Ferreira MZJ, Alencar AM, Negri EM, Saldiva PHN, et al. Human bronchial epithelial cells exposed in vitro to diesel exhaust particles exhibit alterations in cell rheology and cytotoxicity associated with decrease in antioxidant defenses and imbalance in pro- and anti-apoptotic gene expression. Environ Sci Pollut Res 2016;23:9862–9870. Available at: http://link.springer.com/10.1007/s11356-016-6228-x.
5. Dinardo CL, Venturini G, Zhou EH, Watanabe IS, Campos LCG, Dariolli R, da Motta-Leal-Filho JM, Carvalho VM, Cardozo KHM, Krieger JE, et al. Variation of mechanical properties and quantitative proteomics of VSMC along the arterial tree. Am J Physiol Heart Circ Physiol 2014;306:H505–H516. Available at: http://www.ncbi.nlm.nih.gov/pubmed/24337458 (accessed on March 26, 2014).
6. Dinardo CL, Santos HC, Vaquero AR, Martelini AR, Dallan LAO, Alencar AM, Krieger JE, Pereira AC. Smoking and female sex: Independent predictors of human vascular smooth muscle cells stiffening Kirchmair R, editor. PLoS One 2015;10:e0145062. Available at: http://dx.plos.org/10.1371/journal.pone.0145062.
7. Alencar AM, Ferraz MSA, Park CY, Millet E, Trepat X, Fredberg JJ, Butler JP. Non-equilibrium cytoquake dynamics in cytoskeletal remodeling and stabilization. Soft Matter 2016;12:8506–8511. Available at: http://xlink.rsc.org/?DOI=C6SM01041E.
8. Zhou EH, Martinez FD, Fredberg JJ. Cell rheology: Mush rather than machine. Nat Mater 2013;12:184–185. Available at:http://www.pubmedcentral.nih.gov/articlerender.fcgi?artid=3882307&tool=pmcentrez&rendertype=abstract (accessed on January 29, 2014).
9. Fabry B, Maksym G, Butler J, Glogauer M, Navajas D, Fredberg J. Scaling the microrheology of living cells. Phys Rev Lett 2001;87:148102–148104. Available at: http://link.aps.org/doi/10.1103/PhysRevLett.87.148102 (accessed on November 1, 2012).
10. Fletcher DA, Mullins RD. Cell mechanics and the cytoskeleton. Nature 2010;463:485–492. Available at: http://www.nature.com/doifinder/10.1038/nature08908.
11. Alford PW, Nesmith AP, Seywerd JN, Grosberg A, Parker KK. Vascular smooth muscle contractility depends on cell shape. Integr Biol 2011;3:1063–1070. Available at: http://www.ncbi.nlm.nih.gov/pubmed/21993765 (accessed on February 24, 2014).
12. Li F, Yin Z, Jin G, Zhao H, Wong STC. Chapter 17: Bioimage Informatics for Systems Pharmacology Lewitter F, Kann M, editors. PLoS Comput Biol 2013;9:e1003043. Available at: http://www.pubmedcentral.nih.gov/articlerender.fcgi?artid=3635992&tool=pmcentrez&rendertype=abstract (accessed on August 19, 2013).
13. Russ JC. The Image Processing Handbook. Boca Raton, FL: CRC Press; 2010. 180 p.
14. Yoshigi M, Clark EB, Yost HJ. Quantification of stretch-induced cytoskeletal remodeling in vascular endothelial cells by image processing. Cytometry A 2003;55A:109–118.
15. Wong KYE, Chekima A, Dargham JA, Sainarayanan G. Palmprint identification using Sobel operator. In: 10th International Conference on Control, Automation, Robotics and Vision, 2008. ICARCV 2008. Hanoi, Vietnam: IEEE; 2008. pp 1338–1341. Available at: http://ieeexplore.ieee.org/document/4795716/.
16. Xu F, Beyazoglu T, Hefner E, Gurkan UA, Demirci U. Automated and adaptable quantification of cellular alignment from microscopic images for tissue engineering applications. Tissue Eng. C. Methods 2011;17:641–649. Available at: http://www.pubmedcentral.nih.gov/articlerender.fcgi?artid=3103056&tool=pmcentrez&rendertype=abstract.
17. Kemeny SF, Clyne AM. A simplified implementation of edge detection in MATLAB is faster and more sensitive than fast fourier transform for actin fiber alignment quantification. Microsc Microanal 2011;17:156–166.
18. Mangell P, Länne T, Sonesson B, Hansen F, Bergqvist D. Regional differences in mechanical properties between major arteries—An experimental study in sheep. Eur J Vasc Endovasc Surg 1996;12:189–195. Available at: http://www.ncbi.nlm.nih.gov/pubmed/8760981.
19. Peterson LH, Jensen RE, Parnell J. Mechanical properties of arteries in vivo. Circ Res 1960;8:622–639.
20. Dinardo CL, Venturini G, Omae SV, Zhou EH, da Motta-Leal-Filho JM, Dariolli R, Krieger JE, Alencar AM, Costa Pereira A. Vascular smooth muscle cells exhibit a progressive loss of rigidity with serial culture passaging. Biorheology 2012;49:365–373.
21. Doan MXQ, Sarvari AK, Fischer-Posovszky P, Wabitsch M, Balajthy Z, Fesus L, Bacso Z. High content analysis of differentiation and cell death in human adipocytes. Cytometry A 2013;83:933–943.
22. Jin-Yu Z, Yan C, Xian-Xiang H. Edge detection of images based on improved Sobel operator and genetic algorithms. In: International Conference on Image Analysis and Signal Processing, IASP 2009. Linhai, China, China: IEEE; 2009. pp 31–35.
23. Shah SA, Santago P, Rubin BK. Quantification of biopolymer filament structure. Ultramicroscopy 2005;104:244–254.
24. Parameswaran H, Majumdar A, Ito S, Alencar AM, Suki B. Quantitative characterization of airspace enlargement in emphysema. J Appl Physiol 2006;100:186–193.
25. Chinga G, Johnsen PO, Dougherty R, Berli EL, Walter J. Quantification of the 3D microstructure of SC surfaces. J Microsc 2007;227:254–265.
26. Isnard RN, Pannier BM, Laurent S, London GM, Diebold B, Safar ME. Pulsatile diameter and elastic modulus of the aortic arch in essential hypertension: A noninvasive study. J Am Coll Cardiol 1989;13:399–405.
27. Labropoulos N, Ashraf MM, Kang SS, Oh DS, Buckman J, Baker WH. Viscoelastic properties of normal and atherosclerotic carotid arteries. Eur J Vasc Endovasc.Surg 2000;19:221–225.
28. Slørdahl SA, Piene H, Linker DT, Vik A. Segmental aortic wall stiffness from intravascular ultrasound at normal and subnormal aortic pressure in pigs. Acta Physiol Scand 1991;143:227–232. Available at: http://doi.wiley.com/10.1111/j.1748-1716.1991.tb09226.x.
29. Baltgaile G. Arterial wall dynamics. Perspect Med 2012;1:146–151. Available at: http://linkinghub.elsevier.com/retrieve/pii/S2211968X12000563.